Anterior Segment Optical Coherence Tomography

1

Benjamin Y. Xu, Jing Shan, Charles DeBoer, and Tin Aung

Introduction

Anterior segment optical coherence tomography (AS-OCT) is a relatively new in vivo imaging method that acquires cross-sectional images of the anterior segment and its structures by measuring their optical reflections [1]. AS-OCT devices have rapidly evolved over the past decade, integrating newer forms of OCT technology to improve imaging resolution and speed. Over that time, AS-OCT imaging has increased in popularity among clinicians and researchers, especially as a means of studying the anatomy and biomechanics of the anterior segment and its anatomical structures. However, there are few resources that teach the basics of qualitative and quantitative interpretation of AS-OCT images. This chapter acts as a guide for novice AS-OCT image graders while also providing the reader with information on OCT technology, clinical applications of AS-OCT imaging, and future directions of scientific research.

AS-OCT Technologies and Devices

AS-OCT imaging produces cross-sectional or volumetric scans of tissues in vivo or in vitro with micrometer resolution. Optical coherence tomography (OCT) technology is somewhat analogous to ultrasound technology, except that it utilizes light waves rather than sound waves to scan tissues. OCT technology relies on the principle of backscattered light, which is light that originates from a source and is reflected as it passes through materials or tissues. Backscattered light is detected by a sensor, which compares it to a reference light beam. The delay between the two beams provides information about the optical properties of the imaged material or tissue and defines boundaries between nonhomogeneous structures. In the eye, OCT image resolution and depth of penetration vary based on source light intensity and attenuation by intervening tissue structures. There are three commer-

B. Y. Xu (✉)
USC Roski Eye Institute, Keck Medicine of University of Southern California, Los Angeles, CA, USA

Department of Ophthalmology, Keck School of Medicine of University of Southern California, Los Angeles, CA, USA
e-mail: benjamix@usc.edu

J. Shan · C. DeBoer
USC Roski Eye Institute, Keck Medicine of University of Southern California, Los Angeles, CA, USA

Department of Ophthalmology, LAC+USC Medical Center, Los Angeles, CA, USA

T. Aung
Singapore Eye Research Institute, Singapore National Eye Centre, Singapore, Singapore

R. Varma et al. (eds.), *Advances in Ocular Imaging in Glaucoma*, Essentials in Ophthalmology,
https://doi.org/10.1007/978-3-030-43847-0_1

cially available OCT technologies that have been applied to AS-OCT imaging: time-domain OCT and Fourier-domain OCT, which can be subdivided into spectral-domain OCT and swept-source OCT.

The earliest AS-OCT devices were based on time-domain OCT technology. Due to limitations in time-domain OCT technology, early AS-OCT devices such as the Zeiss Visante (Carl Zeiss Meditec, Dublin, CA) and Heidelberg SL-OCT (Heidelberg Engineering, Heidelberg, Germany) had to sacrifice acquisition speed for spatial resolution [2]. These devices also used longer, 1310 μm wavelength light in order to increase imaging depth. As a result, images tended to be noisy and fine details of ocular structures, such as the trabecular meshwork, could not be resolved. In addition, the majority of early AS-OCT studies of the anterior segment were limited to a single cross-sectional OCT image acquired along the horizontal, temporal-nasal meridian. Finally, studies of early time-domain OCT devices reported poorer reliability and reproducibility compared to modern Fourier-domain OCT devices [3–8].

Fourier-domain OCT provides improvements in image quality and acquisition speed compared to time-domain OCT. Spectral-domain OCT devices such as the Zeiss Cirrus (Carl Zeiss Meditec, Dublin, CA) and Heidelberg Spectralis (Heidelberg Engineering, Heidelberg, Germany) utilize shorter wavelength light to produce images with enhanced spatial resolution, although this comes at the cost of imaging depth. This improvement enables more consistent visualization of Schlemm's canal and distal aqueous outflow structures on AS-OCT images. However, both devices require specialized lenses to acquire images that span the width of the anterior chamber. The Tomey CASIA SS-1000 (Tomey Corporation, Nagoya, Japan) is a swept-source Fourier-domain AS-OCT device that can acquire up to 128 cross-sectional OCT images in less than 2 seconds. However, due to its longer 1310 μm wavelength, its spatial resolution lags behind spectral-domain devices. Due to an overall increase in AS-OCT imaging speed, the convention has shifted toward acquiring an increased number of images per eye. This change in methodology has been shown to increase the accuracy of AS-OCT imaging in terms of capturing anatomical variations inherent to the angle [9, 10].

Fourier-domain AS-OCT devices demonstrate excellent intra-examiner and inter-examiner reproducibility of measurements based on the location of the scleral spur or Schwalbe's line [11–15]. However, the correlation between measurements obtained on different devices varies depending on the parameter, ranging from poor to excellent [12, 14]. This difference likely arises from how different devices account for corneal refraction, which is a parameter used to scale and dewarp the corresponding OCT B-scans. Therefore, AS-OCT measurements should not be directly compared or used interchangeably between different devices.

The Iridocorneal Angle: Role in Aqueous Outflow and Assessment Methods

The irideocorneal angle is a key component of the conventional aqueous outflow pathway and plays a crucial role in the development of elevated intraocular pressure (IOP) and glaucomatous optic neuropathy. Aqueous humor is produced by the ciliary body and secreted into the posterior chamber (Fig. 1.1). From the posterior chamber, the aqueous humor flows through the iridolenticular junction, around the iris sphincter, and into the anterior chamber. From there it must pass through the iridocorneal angle to gain access the trabecular meshwork and distal outflow structures. The configuration of the iridocorneal angle and its constituent structures plays an important role in facilitating or impeding the flow of aqueous along this pathway. Appositional contact between the iris and trabecular meshwork can inhibit normal aqueous outflow, thereby leading to elevations of IOP, an important risk factor for the development of glaucomatous optic neuropathy.

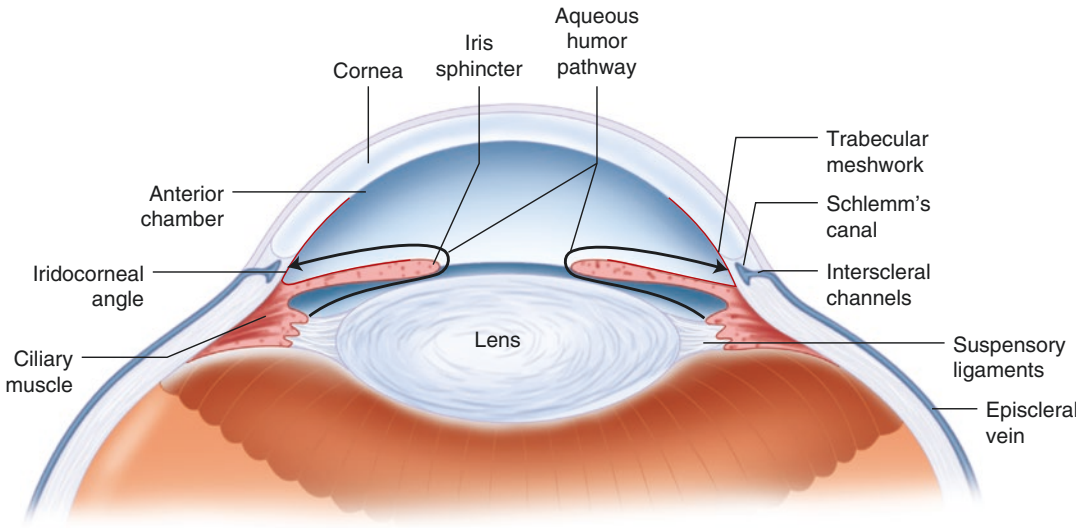

Fig. 1.1 Cross-sectional diagram of the anterior segment. Black arrows indicates the conventional aqueous outflow pathway from the ciliary muscle, around the iris sphincter, into the anterior chamber, and through the iridocorneal angle, trabecular meshwork, Schlemm's canal, interscleral (collector) channel, aqueous vein, and episcleral vein. Red line indicates the iridocorneal angle formed by anterior iris and posterior corneoscleral surfaces

AS-OCT imaging has modernized examination of the anterior segment, including the iridocorneal angle. However, to understand the clinical utility of AS-OCT imaging in glaucoma, it is necessary to discuss gonioscopy and ultrasound biomicroscopy (UBM), two angle assessment methods that preceded AS-OCT.

Gonioscopy is the current clinical standard for evaluating the iridocorneal angle (Fig. 1.2). Gonioscopy is a contact assessment method and requires that a specialized lens be placed on the corneal surface. The goniolens permits a view of the iridocorneal angle either through direct examination, in the case of a direct goniolens (e.g., Koeppe), or indirect examination through a mirror, in the case of indirect goniolenses (e.g., Posner-Zeiss, Goldmann). Indirect gonioscopy is typically preferred over direct gonioscopy since it can be performed with the patient seated at a slit lamp, which increases viewing stability and allows for image magnification. Gonioscopy is also the current clinical standard for detecting angle closure, defined as inability to visualize the pigmented trabecular meshwork, and primary angle closure disease (PACD), defined as gonioscopic angle closure in three or more angle quadrants [16].

Gonioscopy has several limitations despite being the current clinical standard. Gonioscopy is a subjective assessment method requiring considerable examiner expertise. Special attention must be paid to ensure the slit beam does not cross the pupillary margin, which can cause pupillary constriction and widening of the iridocorneal angle. Indentation of the cornea by the goniolens can also induce angle widening or corneal striae, both of which affect the visibility of angle structures. Gonioscopy is also associated with high interobserver variability, even among experienced glaucoma specialists [17]. These differences may be related to patient eye deviations or degree of lens tilting by the examiner, which are aspects of gonioscopy that are difficult to quantify or standardize across examinations. Finally, gonioscopy is a qualitative assessment method. While numerical grades are often assigned to angle quadrants based on identification of anatomical landmarks, these numbers are subjective and categorical in nature. Therefore, there are limited clinical methods based on gonioscopy to track progression of

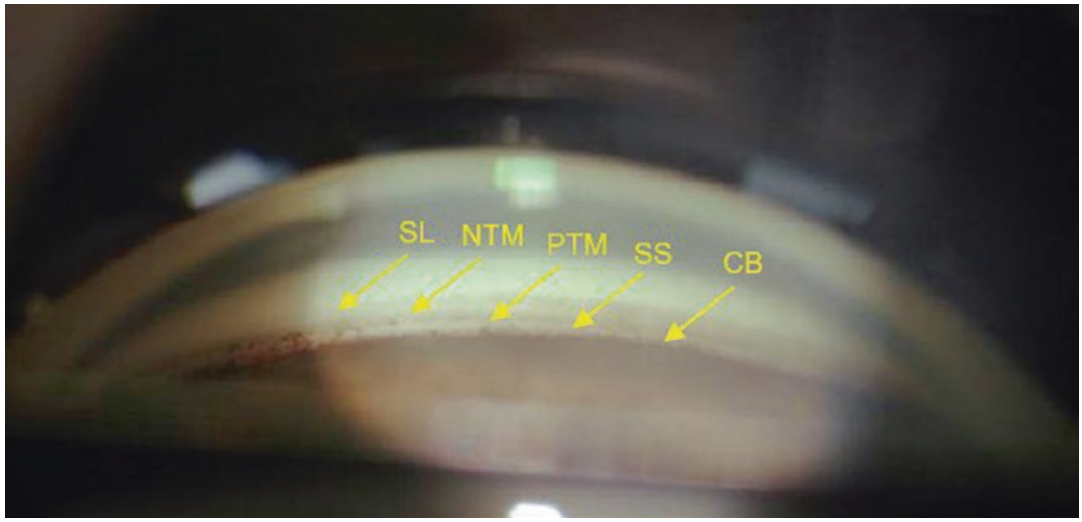

Fig. 1.2 A gonioscopic view of an open iridocorneal angle. Arrows indicate Schwalbe's line (SL), non-pigmented trabecular meshwork (NTM), pigmented trabecular meshwork (PTM), scleral spur (SS), and ciliary body (CB)

angle closure over time or assess patient response to interventions intended to alleviate angle closure, such as LPI.

UBM is an alternative method to assess the anterior segment and its structures. UBM utilizes sound waves that are shorter in wavelength than those used in conventional ocular ultrasonography, which provides increased spatial resolution at the cost of reduced depth of penetration through the sclera. UBM provides qualitative and quantitative assessments of the anterior segment, including the posterior chamber the ciliary body. However, studies demonstrate variable reproducibility of quantitative measurements of anterior chamber parameters, including those that quantify angle width [18, 19]. UBM is also a contact assessment method requiring a trained, experienced examiner. Therefore, its use is limited primarily to glaucoma practices or tertiary referral centers.

AS-OCT provides several advantages over gonioscopy. AS-OCT imaging does not require contact, thus minimizing test-induced distortions of angle configuration. Nor does it require an experienced examiner, as AS-OCT imaging can be performed by a technician with a limited amount of training. AS-OCT imaging also provides quantitative measurements of the anterior segment and its structures, including the width of the iridocorneal angle. Gonioscopy also provides several advantages over AS-OCT. Gonioscopy can be performed with a goniolens at a slit lamp and does not require expensive, specialized equipment. Certain qualitative exam findings, such as peripheral anterior synechiae (PAS) or neovascularization of the angle (NVA), are easier to detect on gonioscopy than AS-OCT. Finally, the clinical relevance of gonioscopy is well supported by a robust body of literature that defines its role in the detection and management of PACD.

AS-OCT imaging resembles UBM imaging in that both provide qualitative and quantitative assessments of the anterior segment. However, AS-OCT provides several advantages over UBM. One advantage is improved spatial resolution, which allows for more reliable detection of key anatomical landmarks, such as the scleral spur. Another advantage is faster imaging speed since AS-OCT does not require probe movements to image different portions of the angle. A third advantage is its noncontact nature; in the absence of a probe applied to the ocular surface, the subject can fixate on a visual stimulus, thereby stabilizing the eye. The combined effect of these two factors is an increase in inter-observer reproducibility, especially among modern Fourier-domain

OCT devices [3–8]. The primary shortcoming of AS-OCT compared to UBM is its inability to visualize anatomical structures posterior to the iris, including the ciliary body. This limits the utility of AS-OCT in diagnosing certain causes of angle closure, such as plateau iris syndrome and iris or ciliary body neoplasms.

Aqueous Outflow Pathways

AS-OCT imaging has been applied to the study of conventional and nonconventional aqueous outflow pathways. The trabecular meshwork and Schlemm's canal are more easily visible on shorter wavelength spectral-domain OCT devices, such as Cirrus and Spectralis (Fig. 1.3), compared to longer wavelength AS-OCT devices, such as CASIA. These devices permit in vivo 360-degree visualization of the proximal structures of the conventional aqueous outflow pathway [20]. Distal aqueous outflow structures, such as collector channels and aqueous veins, are visible on longer wavelength experimental Fourier-domain AS-OCT devices designed to penetrate through the scleral wall [21–23]. The suprachoroidal component of the nonconventional outflow pathway is visible when there is increased fluid in the space, as in the case of uveal effusion or after glaucoma surgery [24–26].

AS-OCT studies of the conventional aqueous outflow pathway have shed light on possible mechanisms by which medications and surgery lower IOP. For example, in vivo AS-OCT imaging has been used to confirm that pilocarpine increases the lumen size of Schlemm's canal in eyes with and without glaucoma [9]. Dilations of Schlemm's canal are also observable after phacoemulsification surgery, and the magnitudes of dilation are correlated with decreases in IOP [27].

Interpretation of AS-OCT Images

AS-OCT images can be interpreted qualitatively, similar to slit lamp assessments of the anterior chamber and gonioscopic assessments of the iridocorneal angle. Some key structures, such as the cornea, lens, and iris, are easily identifiable in AS-OCT images, even to a novice examiner (Fig. 1.4). However, examining the iridotrabecular angle, formed by the junction between the trabecular meshwork and anterior iris surface, for evidence of angle closure is not as intuitive. The imaging-based definition of angle closure is iridotrabecular contact, which is apposition between the trabecular meshwork and anterior surface of the iris (Fig. 1.5). The visibility of the trabecular meshwork on AS-OCT is dependent on a number of factors, including eye stability and quality of the ocular surface. The trabecular meshwork is also easier to visualize on devices utilizing newer OCT technologies or shorter wavelengths of light, such as the Zeiss Cirrus and Heidelberg Spectralis (Fig. 1.3). However, visualizing the trabecular meshwork, Schlemm's canal, and distal outflow pathways is not necessary to identify appositional angle closure.

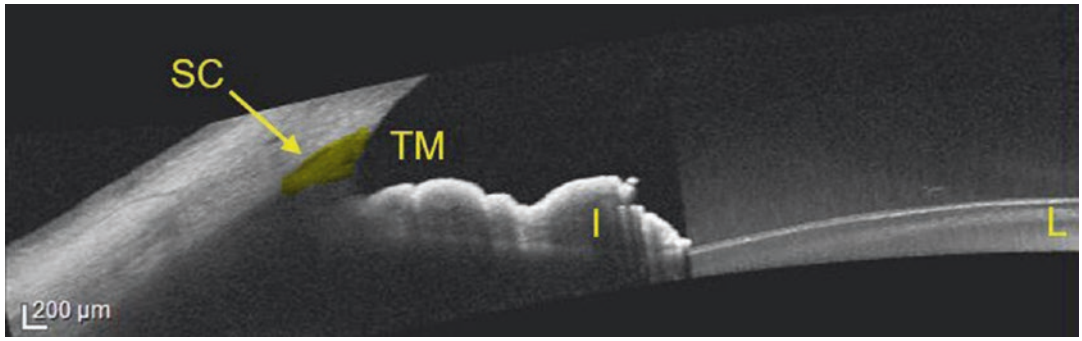

Fig. 1.3 Image taken with the Heidelberg Spectralis with anterior segment module. The iris (I), lens (L), trabecular meshwork (TM), and Schlemm's canal (SC, yellow arrow) are marked

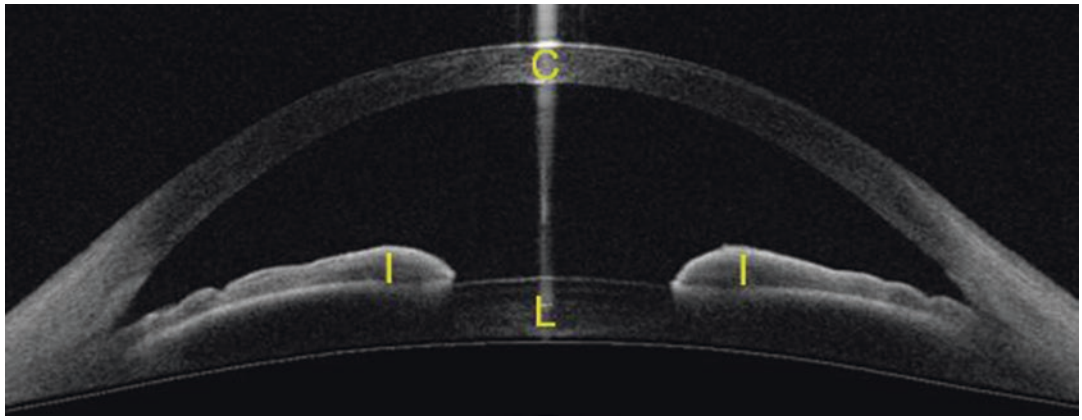

Fig. 1.4 Image taken with the Tomey CASIA SS-1000 demonstrating typical cross-sectional view of the anterior segment along the horizontal, temporal-nasal meridian. The cornea (C), iris (I), and lens (L) are marked

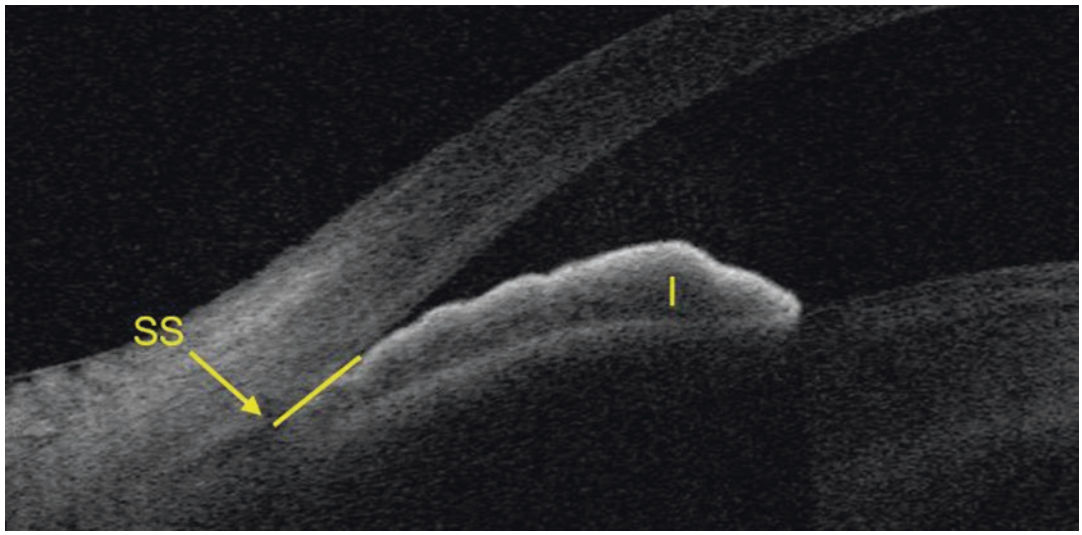

Fig. 1.5 Image taken with the Tomey CASIA SS-1000 demonstrating angle closure. Scleral spur (SS, yellow arrow), iris (I), and segment of iridotrabecular contact (yellow line) are marked

Anatomically, the trabecular meshwork is bounded anteriorly by Schwalbe's line and posteriorly by the scleral spur. As angle closure tends to start posteriorly near the iris root and progress anteriorly, the key anatomical structure to identify in the interpretation of AS-OCT images is the scleral spur. The scleral spur lies at the junction of the trabecular meshwork and ciliary body. On AS-OCT images, the scleral spur is defined as the inward protrusion of the sclera where a change in curvature of the corneoscleral junction is observed (Fig. 1.6) [28]. One AS-OCT study found the average width of the trabecular meshwork ranges between 712 and 889 μm in width depending on the portion of the angle being imaged [29]. Therefore, AS-OCT parameters developed to measure angle width typically focus on a region 250 to 1000 μm anterior to the scleral spur.

Schwalbe's line has been proposed as an alternative to the scleral spur as a reference landmark for measuring AS-OCT parameters [30, 31]. Schwalbe's line is more visible and reliably identified on spectral-domain AS-OCT imaging (Fig. 1.7) [7]. In addition, parameters such as

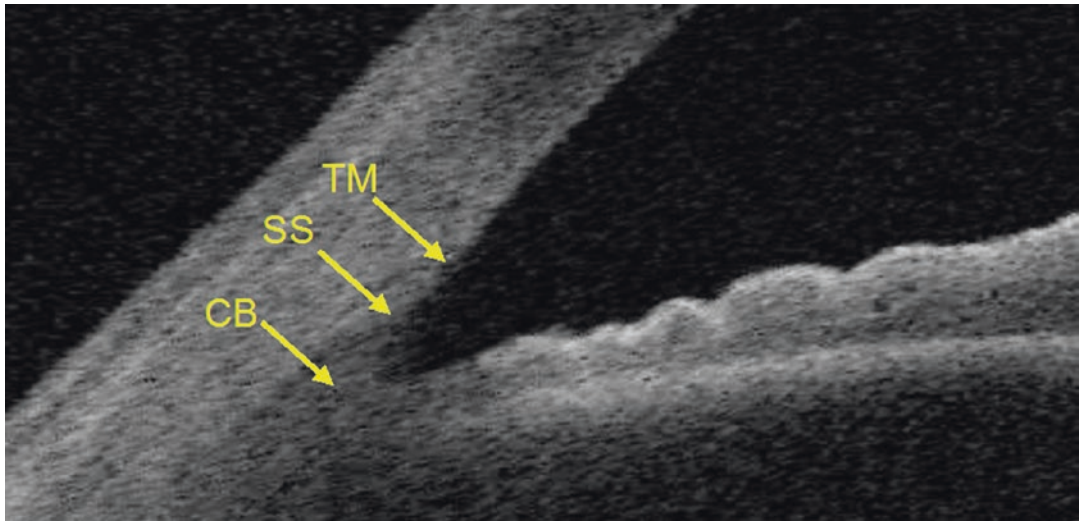

Fig. 1.6 Image taken with the Tomey CASIA SS-1000 demonstrating the scleral spur (SS) located at the junction of the trabecular meshwork (TM) and ciliary body (CB)

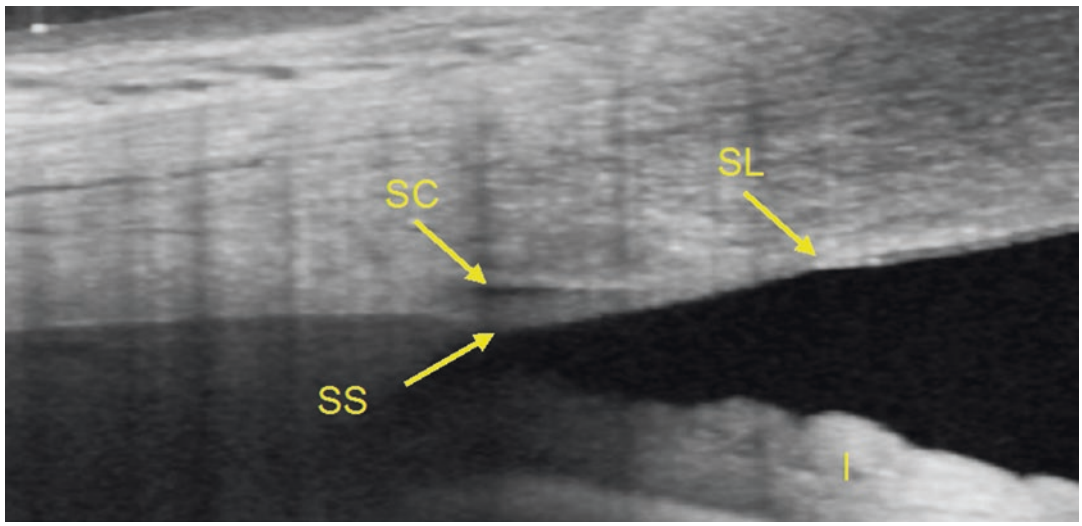

Fig. 1.7 Image taken with the Heidelberg Spectralis with anterior segment module. The iris (I), Schwalbe's line (SL, yellow arrow), Scleral spur (SS, yellow arrow) and Schlemm's canal (SC, yellow arrow) are marked

AOD measured at the location of Schwalbe's line are highly correlated with gonioscopic angle closure [31, 32]. However, the scleral spur currently remains the reference landmark in the majority of AS-OCT studies, both for historical reasons and given the close proximity of its anatomical location to the trabecular meshwork.

As mentioned previously, the primary objective of the examiner is to identify the scleral spur and assess if there is contact between the iris and corneoscleral junction anterior to this point. It is important to note that angle closure defined in this manner based on AS-OCT images is not equivalent to gonioscopic angle closure, which is typically defined as the inability to visualize pigmented trabecular meshwork on gonioscopy. In fact, there is only weak agreement between AS-OCT and gonioscopy in the detection and assessment of angle closure [4, 33]. Therefore, the two assessment methods should not be used interchangeably.

Rather, AS-OCT imaging provides complementary information to gonioscopy in patients in whom appositional angle closure is suspected.

Detection of the scleral spur is more difficult in eyes with angle closure due to crowding of the iridocorneal angle by iris tissue and attenuation of OCT signal (Fig. 1.8). However, with training and experience, it can be detected at a high rate on modern AS-OCT devices as long as the eyelid is adequately retracted during the time of imaging [7]. Disparities in the detection of angle closure between AS-OCT and gonioscopy likely arise from influences of ocular structures, such as the iris and lens, to visualization of angle structures on gonioscopy (Fig. 1.9). For example, Fig. 1.9 illustrates a case in which angle closure was diagnosed on gonioscopy but was not corroborated by AS-OCT imaging. In this case, there is significant anterior positioning of the lens and bowing of the iris, both of which affect the examiner's ability to visualize the pigmented trabecular meshwork.

AS-OCT images can also be interpreted quantitatively, although this requires specialized software not available on all AS-OCT devices. Some AS-OCT devices, such as the Tomey CASIA, have robust built-in software for measuring the width of the angle, extent of iridotrabecular contact (ITC) anterior to the scleral spur, and dimensions of the anterior chamber and its structures (Fig. 1.10) [34]. Other devices, such as the Heidelberg Spectralis, have more limited measurement tools, although these are not FDA approved for patient care or activated on most devices. On the Tomey CASIA, ocular structures such as the cornea, lens, or iris must first be delineated, either automatically by the software or manually by the user. Then, the scleral spur must be marked before measurements of AS-OCT parameters can be computed. This process tends to be time-consuming, which has limited the clinical utility of quantitative AS-OCT measurements. In addition, there is currently no commercially available software for computing AS-OCT

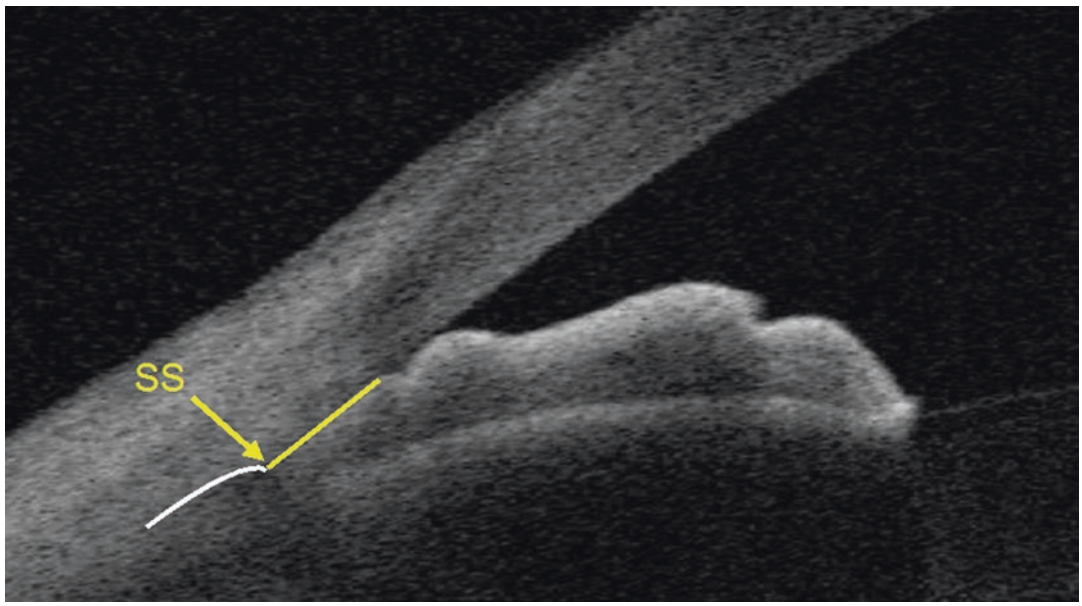

Fig. 1.8 Image taken with the Tomey CASIA SS-1000 demonstrating difficulty of identifying the scleral spur in an eye with angle closure. The scleral spur (SS, yellow arrow), segment of iridotrabecular contact (yellow line), and faint outline of the junction between the sclera and ciliary body (white line) are marked

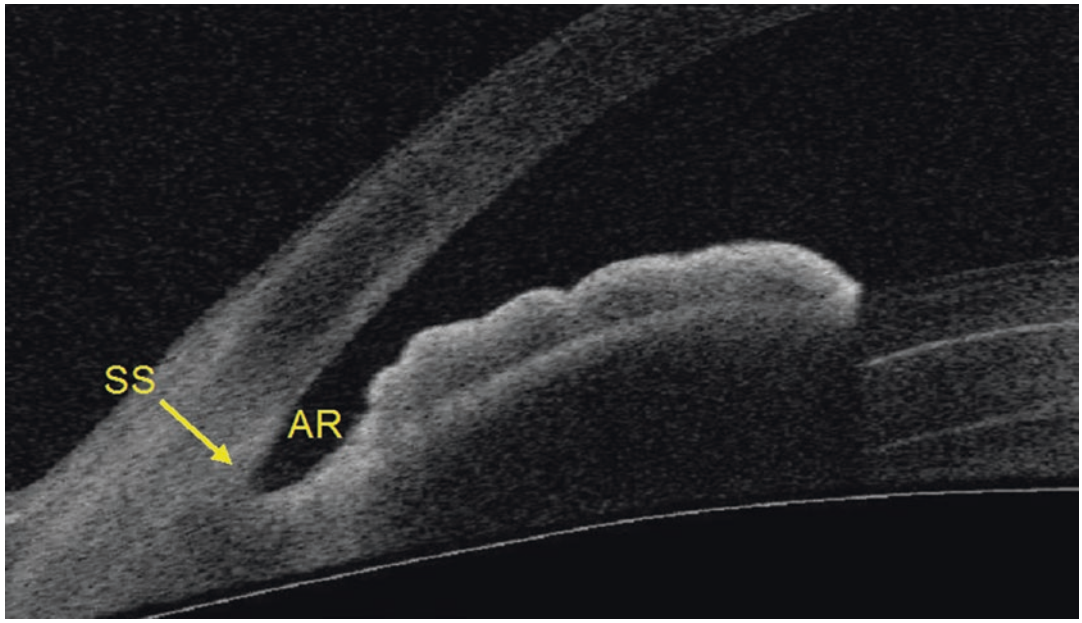

Fig. 1.9 Image taken with the Tomey CASIA SS-1000 demonstrating a lack of iridotrabecular contact in the angle recess (AR) anterior to the scleral spur (SS, yellow arrow) in angle quadrant diagnosed with gonioscopic angle closure

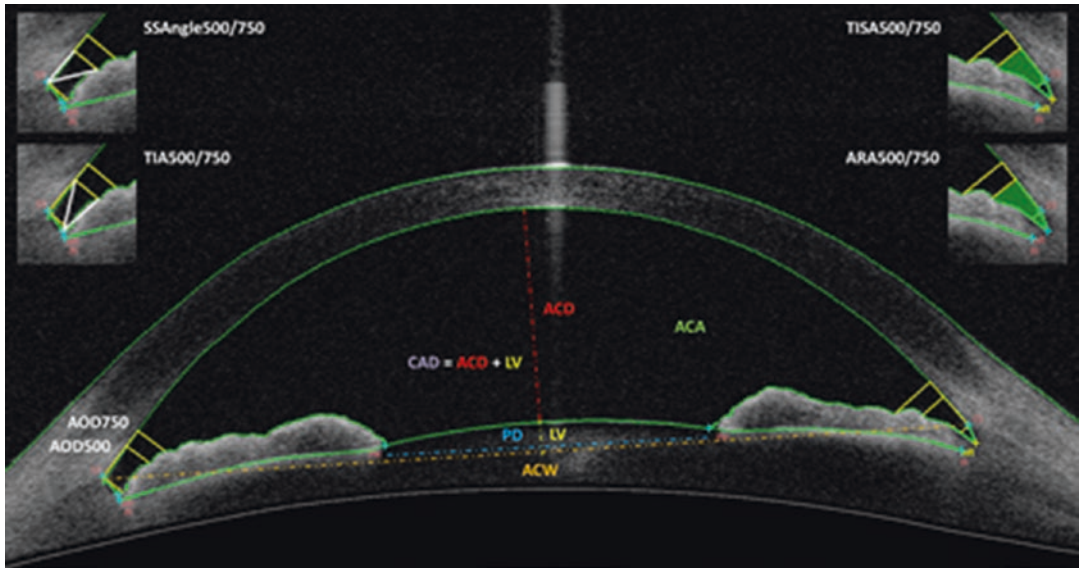

Fig. 1.10 Anterior segment parameters measured by Tomey CASIA SS-1000 using manufacturer-provided software. AOD: angle opening distance. ARA: angle recess area. TIA: trabecular iris angle. TISA: trabecular iris space area. SSAngle: scleral spur angle. ACD: anterior chamber depth. LV: lens vault. CAD: corneal arcuate distance. ACW: anterior chamber width. PD: pupillary diameter. ACA: anterior chamber area. 500 and 750 denote distance from scleral spur in μm

measurements from a variety of AS-OCT devices. AS-OCT studies of the iridocorneal angle reveal significant anatomical variation [10]. While most of this anatomical variation is missed by a single cross-sectional image along the horizontal temporal-nasal meridian, it is captured by as few as four OCT images on average [9, 10]. Therefore, a multi-image analysis approach is recommended for quantitative studies of angle width.

AS-OCT parameters have been devised to describe the dimensions of the iridocorneal angle (Fig. 1.10). The most commonly measured angle parameters include angle opening distance (AOD), angle recess area (ARA), trabecular iris space area (TISA), trabecular iris angle (TIA), and scleral spur angle (SSA) measured at 500 and 750 μm from the scleral spur. AOD is calculated as the perpendicular distance measured from the trabecular meshwork at 500 or 750 μm anterior to the scleral spur to the anterior iris surface. ARA is the area of the angle recess bounded anteriorly by the AOD. TISA is an area bound anteriorly by AOD, posteriorly by a line drawn from the scleral spur perpendicular to the plane of the inner scleral wall to the opposing iris, superiorly by the inner corneoscleral wall, and inferiorly by the iris surface. TIA and SSA are defined as an angle measured with the apex in the iris recess or at the scleral spur, respectively, and the arms of the angle passing through a point on the trabecular meshwork 500 or 750 μm from the scleral spur and the point on the iris perpendicularly. Parameters measuring angle width have a direct relationship with gonioscopy grades or PACD status, although this relationship differs between eyes with open angles and angle closure [35, 36]. Other AS-OCT parameters that describe the dimensions of the anterior chamber and its structures, such as lens vault (LV) and anterior chamber area (ACA), have been identified as biometric risk factors for PACD. These will be discussed in the next section *Biometric Risk Factors for Angle Closure.*

When performing AS-OCT imaging, there are two important factors to take into account: standardization of lighting conditions and retraction of the eyelid. Pupil diameter, a strong determinant of angle width, is affected by environmental lighting conditions due to the pupillary light reflex. Small changes in pupil size can have large effects on angle width measured by AS-OCT [37]. Therefore, it is important to standardize lighting conditions, if not pupil size, during AS-OCT imaging. In addition, inadequate retraction of the eyelid can lead to attenuation of signal, which makes it difficult or impossible to identify the anatomical structures of the iridocorneal angle (Fig. 1.11).

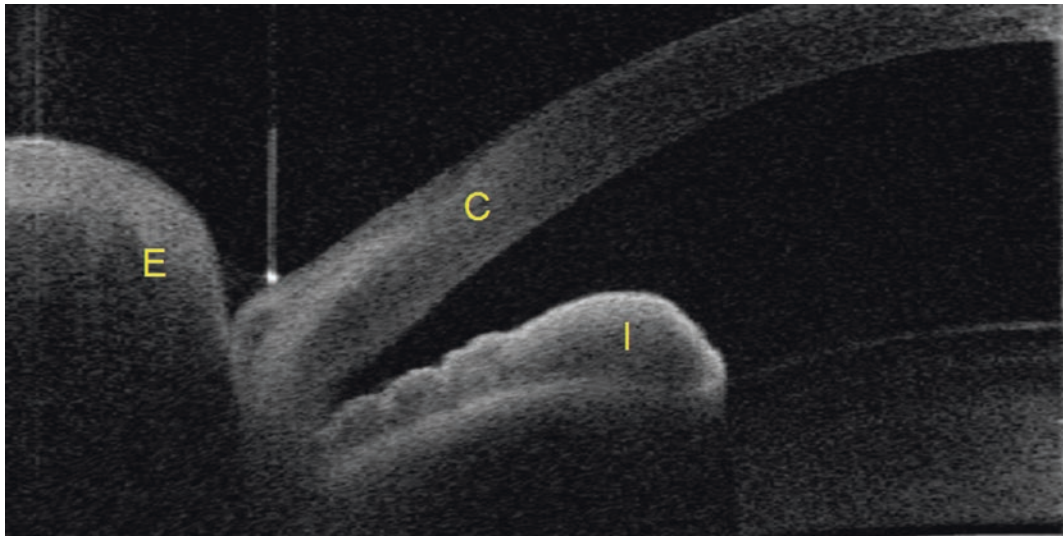

Fig. 1.11 Image taken with the Tomey CASIA SS-1000 demonstrating effect of inadequate eyelid retraction during time of imaging. Eyelid (E), cornea (C), and iris (I) are marked. The scleral spur cannot be reliably identified in this image

Biometric Risk Factors for Angle Closure

Angle closure refers to mechanical obstruction of the trabecular meshwork by the peripheral iris. Angle closure leads to impaired aqueous outflow and elevations in IOP, a strong risk factor for glaucomatous optic neuropathy. Primary angle closure disease (PACD) broadly refers to individuals at risk for this process and is typically divided based on the following gonioscopic classification system [38].

- Primary angle closure suspect (PACS), defined as having gonioscopic angle closure in three or more quadrants without evidence of trabecular meshwork dysfunction or glaucomatous optic neuropathy
- Primary angle closure (PAC), defined as PACS with peripheral anterior synechiae (PAS), excessive pigment deposition on the trabecular meshwork, or elevated IOP > 21 mmHg
- Primary angle closure glaucoma (PACG), defined as PAC with glaucomatous optic neuropathy

Angle parameters that directly measure angle width are intuitive risk factors for gonioscopic angle closure and PACD. However, studies have also identified non-angle parameters that are associated with angle closure. These biometric risk factors can be divided into two categories: static, which comprise measurements derived from individual AS-OCT images, and dynamic, which are measurements computed by comparing measurements from two AS-OCT images, typically obtained under different environmental conditions. Static risk factors include lens vault, anterior chamber area and volume, and iris thickness, area, and curvature [39–44]. Dynamic risk factors include changes in iris area in response to changes in pupil diameter [42–44].

Static Risk Factors

The strongest and most consistently reported static risk factor for gonioscopic angle closure is lens vault (LV), defined as the perpendicular distance separating the anterior pole of the lens from an imaginary horizontal line joining the two scleral spurs [39–42]. Larger values of lens vault are suggestive of increased crowding of the anterior chamber and iridocorneal angle by a thicker or more anterior lens (Fig. 1.12). One study examining angle closure in Chinese subjects reported a

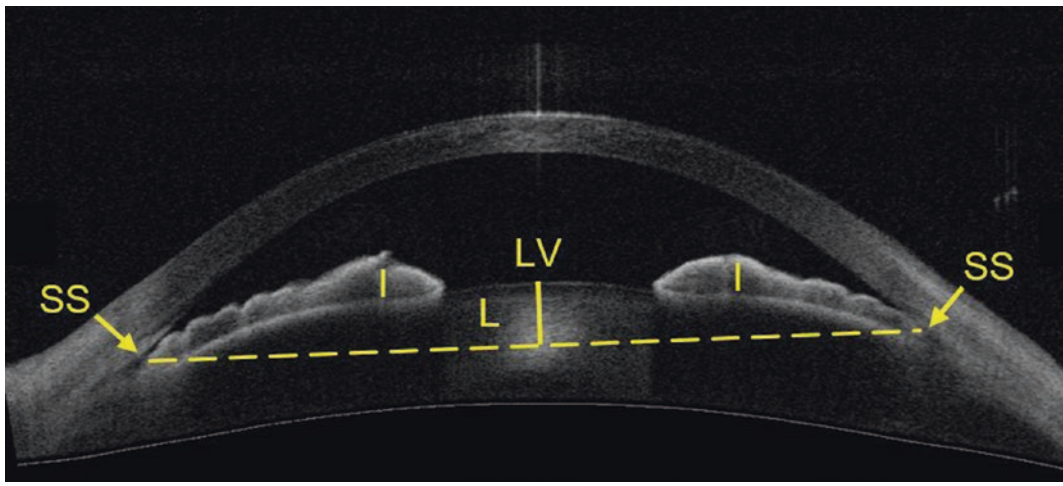

Fig. 1.12 Image taken with the Tomey CASIA SS-1000 demonstrating eye with increased lens vault and angle closure. The iris appears anteriorly bowed and draped over the lens. Scleral spurs (SS), scleral spur plane (dashed yellow line), iris (I), lens (L), and lens vault (LV, yellow line) are marked

significant correlation between gonioscopic angle closure and lens vault [39]. Specifically, eyes in the highest quartile of lens vault measurements were at 48 times higher risk of angle closure compared to subjects in the lowest quartile. This association was independent of known non-biometric risk factors, such as age and gender, as well as other biometric risk factors, such as anterior chamber depth, lens thickness, and relative lens position. These findings were corroborated by a study of Japanese subjects, which reported an odds ratio of 24.2 for angle closure when comparing the lowest and highest quartiles of lens vault measurements [40].

A number of iris-related AS-OCT parameters have also been described as biometric risk factors for angle closure [41–43]. Iris thickness (IT), defined as the largest perpendicular distance along the iris connecting the anterior and posterior iris borders, was found to have an odds ratio of 2.2–2.7 for angle closure when compared with normal eyes. Iris curvature (IC), defined as the perpendicular distance between the iris pigment epithelium and an imaginary line connecting the most peripheral and most central points of iris pigment epithelium, at the point of greatest convexity, and iris area (IA), defined as the cross-sectional area of the full length of the iris, were found to have odds ratios of 0.4–2.5 and 1.1–2.7, respectively.

AS-OCT measurements describing the anterior chamber have also been studied as biometric predictors for angle closure disease. Smaller anterior chamber area (ACA), defined as the cross-sectional area bounded by the corneal endothelium, anterior surface of iris, and anterior surface of lens within the pupil and smaller anterior chamber volume (ACV), calculated by rotating the anterior chamber area 360 degrees around a vertical axis drawn through the midpoint of the anterior chamber, were found to have odds ratios of 53.2 and 40.2, respectively [44]. This translates into 89.9% sensitivity and 85.5% specificity if anterior chamber area measured by AS-OCT is used as a screening parameter for PACD.

Multiparameter models aggregate information provided by multiple biometric risk factors to make predictions on the status of the iridocorneal angle. A six-parameter model based on LV, IA, IT, ACA, ACV, and anterior chamber width (ACW) can generate a probability estimate for gonioscopic angle closure with an area under the receiver operating characteristic curve (AUC) value of 0.94 [49]. A separate longitudinal study that examined the ability of AS-OCT parameters to predicted gonioscopic angle closure reported a model consisting of AOD750 and LV explained 38% of variance in gonioscopic angle closure occurring at 4 years [50]. These results suggest there is a complementary benefit to analyzing multiple biometric risk factors, although there is redundancy in the predictive information they provide.

Dynamic Risk Factors

Dynamic risk factors for angle closure primarily currently focus on changes in the iris associated with pupillary dilation. Studies have shown behaviors of the iris in the transition between light and dark environments differ significantly between open angle and angle closure eyes. Early studies used AS-OCT to quantify and compare the changes in iris area and iris volume associated with pupillary dilation in angle closure versus open angle subjects [45–48]. The results revealed a smaller decrease of iris area and volume with dilation in angle closure eyes compared to open angle eyes.

A more recent study found larger, more peripherally distributed irises increase the risk of post-dilation angle closure [41]. PACS and PACG subjects demonstrated less loss of iris area per millimeter of pupillary distance (PD) increase after physiologic dilation when compared with normal subjects. Regression analysis confirmed that less iris area loss per millimeter PD increase was a significant risk factor for an occludable angle, defined as non-visibility of posterior trabecular meshwork for at least 180 degrees. Furthermore, the change in centroid-to-centroid distance (CCD), defined as the distance between the centers of the nasal and temporal iris masses, per millimeter of PD increase was significantly greater in PACS and PACG subjects compared with normal subjects.

Treatments for Angle Closure and Glaucoma

Glaucoma treatments include lasers procedures and incisional surgeries. More recently, incisional surgery has been subdivided into minimally invasive glaucoma surgery (MIGS) and traditional invasive surgery (e.g., trabeculectomy and glaucoma tube shunts). These interventions are administered in conjunction with medical therapies to control IOP in patients with progressive glaucomatous damage. One role proposed for AS-OCT has been for guiding and evaluating the outcomes of these glaucoma treatments.

Laser peripheral iridotomy (LPI) is typically the first-line intervention in the treatment of angle closure to widen the iridocorneal angle and alleviate angle closure. This procedure utilizes an Nd:YAG laser to create a full-thickness hole in the iris that provides aqueous with an alternative outflow pathway from the posterior chamber to the anterior chamber. LPI significantly increases angle width in angle closure eyes as measured by AS-OCT parameters such as AOD500, TISA500, and ARA500 [51–53]. However, the use of LPI varies widely in early stage PACD as there is no widely held consensus on when it should be performed in the absence of PAS, elevated IOP, or glaucomatous optic neuropathy.

Progressive enlargement of the crystalline lens contributes to pupillary block, the primary mechanism underlying angle closure and PACD. Cataract extraction can widen the angle and lower IOP [54–56]. In angle closure eyes, postsurgical decreases in IOP are primarily due to improved access to the conventional outflow pathway by the aqueous humor. However, AS-OCT studies have also shown that dilations of Schlemm's canal are observable after phacoemulsification surgery, which may explain its IOP-lowering effect even in eyes with open angles [27, 55]. Phacoemulsification combined with goniosynechialysis is often considered as the primary surgical intervention to alleviate angle closure and lower IOP in patients with PACG [57]. The addition of goniosynechialysis provides greater reduction of iridotrabecular contact than phacoemulsification alone, a beneficial effect that can be quantified by AS-OCT. [28]

The well-established gold standard in glaucoma surgery is trabeculectomy, which creates a corneoscleral opening under a partial-thickness scleral flap. This opening serves as an alternate pathway for aqueous outflow from the anterior chamber to the sub-Tenon's and sub-conjunctival spaces, leading to the formation of a bleb. AS-OCT provides detailed visualization of the trabeculectomy bleb (Fig. 1.13), and several stud-

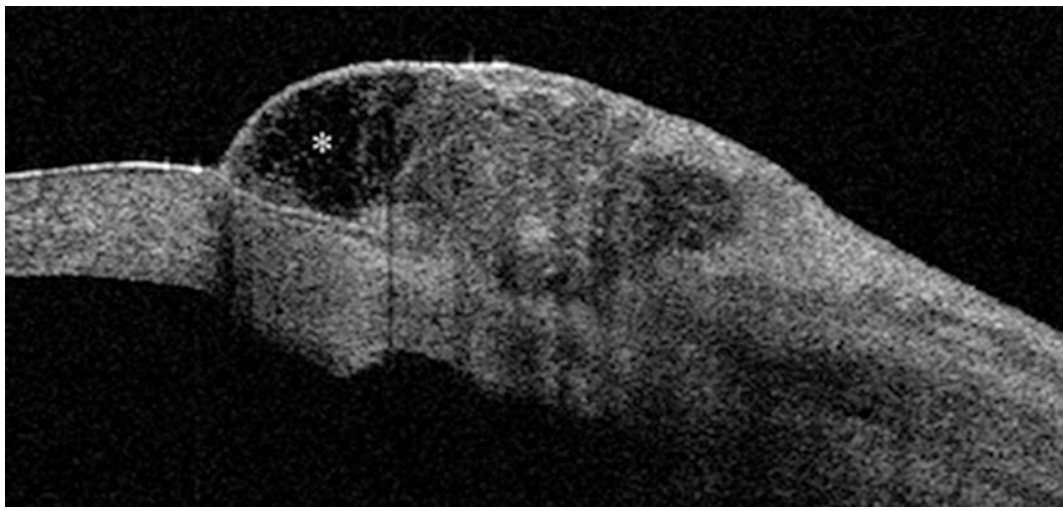

Fig. 1.13 Image taken with the Zeiss Visante demonstrating functioning filtering bleb after MMC-augmented trabeculectomy. The multilobed cystic bleb shows a patent and low reflective fluid-filled inner cavity (asterisk) (Reprinted from Mastropasqua et al., 2014 under a Creative Commons Attribution license [64])

ies have reported an association of bleb morphology with level of IOP control [58–64]. Features of bleb morphology associated with successful IOP lowering include a multilayered appearance and low reflectivity of the bleb wall, presence of episcleral fluid, as well as lower internal reflectivity of the fluid-filled cavity [62, 63]. AS-OCT can also be used to quantify dynamic changes in bleb morphology following laser suture lysis, which can be predictive of long-term surgical outcome [65, 66].

A number of minimally invasive glaucoma surgeries (MIGS) have been introduced over the past decade for the surgical management of glaucoma patients. MIGS devices restore, enhance, or provide an alternative to the eye's natural aqueous outflow pathways by shunting aqueous from the anterior chamber into Schlemm's canal, suprachoroidal space, or sub-Tenon's and subconjunctival spaces. AS-OCT imaging provides a noninvasive method to evaluate short- and long-term postsurgical placement and effect of MIGS in these anatomical structures and spaces [25, 67–70].

Future Directions of Research

AS-OCT technology has rapidly evolved over the past decade. However, the clinical adoption of AS-OCT imaging for the management of PACD has been slow. One reason is there are no automated methods to facilitate the quantitative interpretation of AS-OCT images. Another reason is that clinical and functional significance of angle closure detected by AS-OCT imaging is not as well understood as the significance of angle closure detected by gonioscopy.

The primary advantage of AS-OCT over gonioscopy is it provides quantitative measurements in addition to qualitative assessments of angle width. Automated algorithms support the quantitative analyses of posterior segment structures, such as the retina and optic nerve head. Longitudinal measurements of retinal and nerve fiber layer thickness have modernized the management of posterior segment diseases, allowing clinicians to detect disease progression and response to treatment. In theory, AS-OCT could support similar longitudinal studies of anterior segment diseases. However, quantitative analysis of AS-OCT images is at best semiautomated and requires manual identification of the scleral spur in each image [71]. Experimental automated methods that extract measurements from AS-OCT images by matching them to hand-marked exemplar datasets demonstrated only satisfactory performance [72]. AS-OCT measurements could be used to detect the presence or progression of anterior segment diseases, including PACD [49, 73]. However, clinical adoption of quantitative AS-OCT imaging will likely remain limited until well-performing automated methods have been integrated into mainstream commercial AS-OCT devices.

The current AS-OCT definition of angle closure is based on static structural findings lacking long-term clinical and functional significance. AS-OCT imaging provides three-dimensional information about the structural configuration of the iridocorneal angle, which reflects the amount of access aqueous humor has to the conventional outflow pathway. However, studies exploring this structure-function relationship are limited. One recent study explored the relationship between average angle width measured by AS-OCT and IOP and established threshold values below which angle width and IOP are strongly correlated [74]. However, the degree and extent of iridotrabecular contact required before aqueous outflow and IOP are affected is unknown. Longitudinal studies of angle closure detected on AS-OCT are similarly limited. One study found that in eyes with open angles on baseline examination, iridotrabecular contact detected on AS-OCT was predictive of gonioscopic angle closure after 4 years [75]. Therefore, future research must focus on developing functionally significant definitions of angle closure that are validated through longitudinal clinical studies.

Conclusion

AS-OCT is a noninvasive in vivo imaging method that has gained popularity among clinicians and researchers over the past decade. AS-OCT imag-

ing facilitates qualitative and quantitative studies of the anterior segment and has applications for characterizing anatomical structures, diagnosing and staging disease, and assessing treatment efficacy. However, its adoption in routine clinical care significantly lags behind OCT studies of the posterior segment. Therefore, further work is needed to demonstrate and validate the benefit of novel OCT-based methods compared to current clinical standards of care in the management of anterior segment diseases.

Compliance with Ethical Requirements Benjamin Y. Xu, Jing Shan, Charles DeBoer, and Tin Aung declare that they have no conflicts of interest. No human or animal studies were carried out by the authors for this article.

References

1. Izatt JA, Hee MR, Swanson EA, et al. Micrometer-scale resolution imaging of the anterior eye in vivo with optical coherence tomography. Arch Ophthalmol. 1994;112(12):1584–9.
2. Asrani S, Sarunic M, Santiago C, Izatt J. Detailed visualization of the anterior segment using Fourier-domain optical coherence tomography. Arch Ophthalmol. 2008;126(6):765–71.
3. Liu S, Yu M, Ye C, Lam DSC, Leung CKS. Anterior chamber angle imaging with swept-source optical coherence tomography: An investigation on variability of angle measurement. Investig Ophthalmol Vis Sci. 2011;52(12):8598–603.
4. Sakata LM, Lavanya R, Friedman DS, et al. Comparison of Gonioscopy and anterior segment ocular coherence tomography in detecting angle closure in different quadrants of the anterior chamber angle. Ophthalmology. 2008;115(5):769–74.
5. Sharma R, Sharma A, Arora T, et al. Application of anterior segment optical coherence tomography in glaucoma. Surv Ophthalmol. 2014;59(3):311–27.
6. Maram J, Pan X, Sadda S, Francis B, Marion K, Chopra V. Reproducibility of angle metrics using the time-domain anterior segment optical coherence tomography: intra-observer and inter-observer variability. Curr Eye Res. 2015;40(5):496–500.
7. McKee H, Ye C, Yu M, Liu S, Lam DSC, Leung CKS. Anterior chamber angle imaging with swept-source optical coherence tomography: detecting the scleral spur, Schwalbe's line, and Schlemm's canal. J Glaucoma. 2013;22(6):468–72.
8. Pan X, Marion K, Maram J, et al. Reproducibility of anterior segment angle metrics measurements derived from cirrus spectral domain optical coherence tomography. J Glaucoma. 2015;24(5):e47–51.
9. Blieden LS, Chuang AZ, Baker LA, et al. Optimal number of angle images for calculating anterior angle volume and iris volume measurements. Investig Ophthalmol Vis Sci. 2015;56(5):2842–7.
10. Xu BY, Israelsen P, Pan BX, Wang D, Jiang X, Varma R. Benefit of measuring anterior segment structures using an increased number of optical coherence tomography images: the Chinese American Eye Study. Investig Ophthalmol Vis Sci. 2016;57(14):6313–9.
11. Aptel F, Chiquet C, Gimbert A, et al. Anterior segment biometry using spectral-domain optical coherence tomography. J Refract Surg. 2014;30(5):354–60.
12. Marion KM, Maram J, Pan X, et al. Reproducibility and agreement between 2 spectral domain optical coherence tomography devices for anterior chamber angle measurements. J Glaucoma. 2015;24(9):642–6.
13. Cumba RJ, Radhakrishnan S, Bell NP, et al. Reproducibility of scleral spur identification and angle measurements using fourier domain anterior segment optical coherence tomography. J Ophthalmol. 2012;2012:1–14.
14. Xu BY, Mai DD, Penteado RC, Saunders L, Weinreb RN. Reproducibility and agreement of anterior segment parameter measurements obtained using the CASIA2 and Spectralis OCT2 optical coherence tomography devices. J Glaucoma. 2017;26(11):974–9.
15. Akil H, Dastiridou A, Marion K, Francis B, Chopra V. Repeatability, reproducibility, agreement characteristics of 2 SD-OCT devices for anterior chamber angle measurements. Can J Ophthalmol. 2017;52(2):166–70.
16. Foster PJ, Aung T, Nolan WP, et al. Defining "occludable" angles in population surveys: drainage angle width, peripheral anterior synechiae, and glaucomatous optic neuropathy in east Asian people. Br J Ophthalmol. 2004;88(4):486–90.
17. Rigi M, Bell NP, Lee DA, et al. Agreement between Gonioscopic examination and swept source Fourier domain anterior segment optical coherence tomography imaging. J Ophthalmol. 2016;2016:1727039.
18. Tello C, Liebmann J, Potash SD, Cohen H, Ritch R. Measurement of ultrasound biomicroscopy images: intraobserver and interobserver reliability. Invest Ophthalmol Vis Sci. 1994;35(9):3549–52.
19. Spaeth GL, Azuara-Blanco A, Araujo SV, Augsburger JJ. Intraobserver and interobserver agreement in evaluating the anterior chamber angle configuration by ultrasound biomicroscopy. J Glaucoma. 1997;6(1):13–7.
20. Huang AS, Belghith A, Dastiridou A, Chopra V, Zangwill LM, Weinreb RN. Automated circumferential construction of first-order aqueous humor outflow pathways using spectral-domain optical coherence tomography. J Biomed Opt. 2017;22(6):66010.
21. Li P, An L, Reif R, Shen TT, Johnstone M, Wang RK. In vivo microstructural and microvascular imaging of the human corneo-scleral limbus using optical coherence tomography. Biomed Opt Express. 2011;2(11):3109–18.

22. Uji A, Muraoka Y, Yoshimura N. In vivo identification of the Posttrabecular aqueous outflow pathway using swept-source optical coherence tomography. Investig Opthalmol Vis Sci. 2016;57(10):4162.
23. Huang AS, Camp A, Xu BY, Penteado RC, Weinreb RN. Aqueous angiography: aqueous humor outflow imaging in live human subjects. Ophthalmology. 2017;124(8):1249–51.
24. Gazzard G, Friedman DS, Devereux J, Sean S. Primary acute angle closure glaucoma associated with suprachoroidal fluid in three Chinese patients. Eye. 2001;15(3):358–60.
25. Saheb H, Ianchulev T, Ahmed IK. Optical coherence tomography of the suprachoroid after CyPass Micro-Stent implantation for the treatment of open-angle glaucoma. Br J Ophthalmol. 2014;98(1):19–23.
26. Vieira L, Noronha M, Lemos V, Reina M, Gomes T. Anterior segment optical coherence tomography imaging of filtering blebs after deep Sclerectomy with Esnoper-clip implant: one-year follow-up. J Curr Glaucoma Pract. 2014;8(3):91–5.
27. Zhao Z, Zhu X, He W, Jiang C, Lu Y. Schlemm's canal expansion after uncomplicated phacoemulsification surgery: an optical coherence tomography study. Investig Ophthalmol Vis Sci. 2016;57(15):6507–12.
28. Ho SW, Baskaran M, Zheng C, et al. Swept source optical coherence tomography measurement of the iris-trabecular contact (ITC) index: a new parameter for angle closure. Graefes Arch Clin Exp Ophthalmol. 2013;251(4):1205–11.
29. Tun TA, Baskaran M, Zheng C, et al. Assessment of trabecular meshwork width using swept source optical coherence tomography. Graefes Arch Clin Exp Ophthalmol. 2013;251(6):1587–92.
30. Cheung CY, Zheng C, Ho C-L, et al. Novel anterior-chamber angle measurements by high-definition optical coherence tomography using the Schwalbe line as the landmark. Br J Ophthalmol. 2011;95(7):955–9.
31. Qin B, Francis BA, Li Y, et al. Anterior chamber angle measurements using Schwalbe's line with high-resolution Fourier-domain optical coherence tomography. J Glaucoma. 2013;22(9):684–8.
32. Cheung CY, Zheng C, Ho CL, et al. Novel anterior-chamber angle measurements by high-definition optical coherence tomography using the Schwalbe line as the landmark. Br J Ophthalmol. 2011;95(7):955–9.
33. Xu BY, Pardeshi AA, Burkemper B, et al. Quantitative evaluation of Gonioscopic and EyeCam assessments of angle dimensions using anterior segment optical coherence tomography. Transl Vis Sci Technol. 2018;7(6):33.
34. Baskaran M, Ho S-W, Tun TA, et al. Assessment of circumferential angle-closure by the iris-trabecular contact index with swept-source optical coherence tomography. Ophthalmology. 2013;120(11):2226–31.
35. Narayanaswamy A, Sakata LM, He MG, et al. Diagnostic performance of anterior chamber angle measurements for detecting eyes with narrow angles: an anterior segment OCT study. Arch Ophthalmol. 2010;128(10):1321–7.
36. Xu BY, Pardeshi AA, Burkemper B, et al. Quantitative evaluation of Gonioscopic and EyeCam assessments of angle dimensions using anterior segment optical coherence tomography. Transl Vis Sci Technol. 2018;7(6):33.
37. Leung CKS, Cheung CYL, Li H, et al. Dynamic analysis of dark-light changes of the anterior chamber angle with anterior segment OCT. Investig Ophthalmol Vis Sci. 2007;48(9):4116–22.
38. Foster PJ, Buhrmann R, Quigley HA, Johnson GJ. The definition and classification of glaucoma in prevalence surveys. Br J Ophthalmol. 2002;86(2):238–42.
39. Nongpiur ME, He M, Amerasinghe N, et al. Lens vault, thickness, and position in Chinese subjects with angle closure. Ophthalmology. 2011;118(3):474–9.
40. Ozaki M, Nongpiur ME, Aung T, He M, Mizoguchi T. Increased lens vault as a risk factor for angle closure: confirmation in a Japanese population. Graefes Arch Clin Exp Ophthalmol. 2012;250(12):1863–8.
41. Zhang Y, Li SZ, Li L, He MG, Thomas R, Wang NL. Dynamic iris changes as a risk factor in primary angle closure disease. Investig Ophthalmol Vis Sci. 2016;57(1):218–26.
42. Wang B, Sakata LM, Friedman DS, et al. Quantitative Iris parameters and association with narrow angles. Ophthalmology. 2010;117(1):11–7.
43. Wang BS, Narayanaswamy A, Amerasinghe N, et al. Increased iris thickness and association with primary angle closure glaucoma. Br J Ophthalmol. 2011;95(1):46–50.
44. Wu RY, Nongpiur ME, He MG, et al. Association of narrow angles with anterior chamber area and volume measured with anterior-segment optical coherence tomography. Arch Ophthalmol. 2011;129(5):569–74.
45. Aptel F, Chiquet C, Beccat S, Denis P. Biometric evaluation of anterior chamber changes after physiologic pupil dilation using Pentacam and anterior segment optical coherence tomography. Investig Ophthalmol Vis Sci. 2012;53(7):4005–10.
46. Aptel F, Denis P. Optical coherence tomography quantitative analysis of Iris volume changes after pharmacologic Mydriasis. Ophthalmology. 2010;117(1):3–10.
47. Quigley HA, Silver DM, Friedman DS, et al. Iris cross-sectional area decreases with pupil dilation and its dynamic behavior is a risk factor in angle closure. J Glaucoma. 2009;18(3):173–9.
48. Seager FE, Jefferys JL, Quigley HA. Comparison of dynamic changes in anterior ocular structures examined with anterior segment optical coherence tomography in a cohort of various origins. Investig Ophthalmol Vis Sci. 2014;55(3):1672–83.
49. Nongpiur ME, Haaland BA, Perera SA, et al. Development of a score and probability estimate for detecting angle closure based on anterior segment optical coherence tomography. Am J Ophthalmol. 2014;157(1):32–38.e1.
50. Nongpiur ME, Aboobakar IF, Baskaran M, et al. Association of baseline anterior segment parameters

with the development of incident Gonioscopic angle closure. JAMA Ophthalmol. 2017;135(3):252–8.
51. Ramakrishnan R, Mitra A, Abdul Kader M, Das S. To study the efficacy of laser peripheral iridoplasty in the treatment of eyes with primary angle closure and plateau iris syndrome, unresponsive to laser peripheral iridotomy, using anterior-segment OCT as a tool. J Glaucoma. 2016;25(5):440–6.
52. Lee KS, Sung KR, Kang SY, Cho JW, Kim DY, Kook MS. Residual anterior chamber angle closure in narrow-angle eyes following laser peripheral iridotomy: anterior segment optical coherence tomography quantitative study. Jpn J Ophthalmol. 2011;55(3):213–9.
53. Radhakrishnan S, Chen PP, Junk AK, Nouri-Mahdavi K, Chen TC. Laser peripheral Iridotomy in primary angle closure: a report by the American Academy of Ophthalmology. Ophthalmology. 2018;125(7):1110–20.
54. Harasymowycz PJ, Papamatheakis DG, Ahmed I, et al. Phacoemulsification and goniosynechialysis in the management of unresponsive primary angle closure. J Glaucoma. 2005;14(3):186–9.
55. Mansberger SL, Gordon MO, Jampel H, et al. Reduction in intraocular pressure after cataract extraction: the ocular hypertension treatment study. Ophthalmology. 2012;119(9):1826–31.
56. Zhang ZM, Niu Q, Nie Y, Zhang J. Reduction of intraocular pressure and improvement of vision after cataract surgeries in angle closure glaucoma with concomitant cataract patients. Int J Clin Exp Med. 2015;8(9):16557–63.
57. Tham CCY, Kwong YYY, Baig N, Leung DYL, Li FCH, Lam DSC. Phacoemulsification versus trabeculectomy in medically uncontrolled chronic angle-closure glaucoma without cataract. Ophthalmology. 2013;120(1):62–7.
58. Singh M, Chew PTK, Friedman DS, et al. Imaging of trabeculectomy blebs using anterior segment optical coherence tomography. Ophthalmology. 2007;114(1):47–53.
59. Savini G, Zanini M, Barboni P. Filtering blebs imaging by optical coherence tomography. Clin Exp Ophthalmol. 2005;33(5):483–9.
60. Inoue T, Matsumura R, Kuroda U, Nakashima KI, Kawaji T, Tanihara H. Precise identification of filtration openings on the scleral flap by three-dimensional anterior segment optical coherence tomography. Investig Ophthalmol Vis Sci. 2012;53(13):8288–94.
61. Nakano N, Hangai M, Nakanishi H, et al. Early trabeculectomy bleb walls on anterior-segment optical coherence tomography. Graefes Arch Clin Exp Ophthalmol. 2010;248(8):1173–82.
62. Pfenninger L, Schneider F, Funk J. Internal reflectivity of filtering blebs versus intraocular pressure in patients with recent trabeculectomy. Investig Ophthalmol Vis Sci. 2011;52(5):2450–5.
63. Tominaga A, Miki A, Yamazaki Y, Matsushita K, Otori Y. The assessment of the filtering bleb function with anterior segment optical coherence tomography. J Glaucoma. 2010;19(8):551–5.
64. Mastropasqua R, Fasanella V, Agnifili L, Curcio C, Ciancaglini M, Mastropasqua L. Anterior segment optical coherence tomography imaging of conjunctival filtering blebs after glaucoma surgery. Biomed Res Int. 2014;2014:610623.
65. Sng CCA, Singh M, Chew PTK, et al. Quantitative assessment of changes in trabeculectomy blebs after laser suture lysis using anterior segment coherence tomography. J Glaucoma. 2012;21(5):313–7.
66. Singh M, Aung T, Friedman DS, et al. Anterior segment optical coherence tomography imaging of trabeculectomy blebs before and after laser suture lysis. Am J Ophthalmol. 2007;143(5):873–5.
67. Ichhpujani P, Katz LJ, Gille R, Affel E. Imaging modalities for localization of an iStent ®. Ophthalmic Surg Lasers Imaging. 2010;41(6):660–3.
68. Lenzhofer M, Strohmaier C, Hohensinn M, et al. Longitudinal bleb morphology in anterior segment OCT after minimally invasive transscleral ab interno Glaucoma Gel Microstent implantation. Acta Ophthalmol. 2018;97(2):e231–7.
69. Fuest M, Kuerten D, Koch E, et al. Evaluation of early anatomical changes following canaloplasty with anterior segment spectral-domain optical coherence tomography and ultrasound biomicroscopy. Acta Ophthalmol. 2016;94(5):e287–92.
70. Kuerten D, Plange N, Becker J, Walter P, Fuest M. Evaluation of long-term anatomic changes following Canaloplasty with anterior segment spectral-domain optical coherence tomography and ultrasound biomicroscopy. J Glaucoma. 2018;27(1):87–93.
71. Console JW, Sakata LM, Aung T, Friedman DS, He M. Quantitative analysis of anterior segment optical coherence tomography images: the Zhongshan Angle Assessment Program. Br J Ophthalmol. 2008;92(12):1612–6.
72. Fu H, Xu Y, Lin S, et al. Segmentation and quantification for angle-closure glaucoma assessment in anterior segment oct. IEEE Trans Med Imaging. 2017;36(9):1930–8.
73. Lavanya R, Foster PJ, Sakata LM, et al. Screening for narrow angles in the Singapore population: evaluation of new noncontact screening methods. Ophthalmology. 2008;115(10):1720–7, 1727.e1-2.
74. Xu BY, Burkemper B, Lewinger JP, et al. Correlation between intraocular pressure and angle configuration measured by OCT. Ophthalmol Glaucoma. 2018;1:158–66.
75. Baskaran M, Iyer JV, Narayanaswamy AK, et al. Anterior segment imaging predicts incident gonioscopic angle closure. Ophthalmology. 2015;122(12):2380–4.